The mechanical property evolution and grain boundary accommodation during hydride transformation in commercial pure titanium

Qian Wang, Jean-Sébastien Lecomte, Christophe Schuman, Auriane Mandrelli

▶ **To cite this version:**

Qian Wang, Jean-Sébastien Lecomte, Christophe Schuman, Auriane Mandrelli. The mechanical property evolution and grain boundary accommodation during hydride transformation in commercial pure titanium. Materials Science and Engineering: A, 2021, 812, pp.141099. 10.1016/j.msea.2021.141099 . hal-03863716

HAL Id: hal-03863716

https://hal-cnrs.archives-ouvertes.fr/hal-03863716

Submitted on 29 Nov 2022

HAL is a multi-disciplinary open access archive for the deposit and dissemination of scientific research documents, whether they are published or not. The documents may come from teaching and research institutions in France or abroad, or from public or private research centers.

L'archive ouverte pluridisciplinaire **HAL**, est destinée au dépôt et à la diffusion de documents scientifiques de niveau recherche, publiés ou non, émanant des établissements d'enseignement et de recherche français ou étrangers, des laboratoires publics ou privés.

The mechanical property evolution and grain boundary accommodation during hydride transformation in commercial pure titanium

Qian Wang [a,b], Jean-Sébastien Lecomte [a,b,*], Christophe Schuman [a,b,**], Auriane Mandrelli[a,b]

[a] Laboratoire d'Etude des Microstructures et de Mécanique des Matériaux (LEM3), Université de Lorraine CNRS, Arts et Métiers ParisTech, Metz 57073, France

[b] Laboratory of Excellence on Design of Alloy Metals for low-mAss Structures (DAMAS), University of Lorraine, Metz 57073, France

***Corresponding author.**

****Corresponding author.**

E-mail adresses: jean-sebastien.lecomte@univ-lorraine.fr

christophe.schuman@univ-lorraine.fr

Abstract

The mechanical property evolution of titanium surface during hydrogen charging was investigated by nanoindentation tests. The nanohardness increases while elastic modulus decreases due to the formation of hydride precipitation. By mean of interrupted in-situ electron backscatter diffraction (EBSD) measurements, the microstructure evolution of hydrogenated surface was examined. The more prevalent grain-boundary accommodation in fine grain sample leads to the faster hydride transformation from γ to stable δ hydride and less distortion than coarse grain sample. The formation of cross-boundary hydride is regarded as one type of grain-boundary accommodation mode. Transgranular hydrides prefer to be induced at grain boundaries with both low ***c***-axis misorientation angle θ_c ($< 30^o$) and high θ_c ($75^o < \theta_c < 85^o$). The synergistic shear of Shockley partial dislocation and the ***c***-axis dilatation misfit of phase transformation respectively are the fundamental reason for the above two types of grain boundaries.

Keywords: Titanium; Hydride; Nanoindentation; EBSD; Grain boundary;

1. Introduction

Ti and its alloys have a variety of application due to their superior properties, including high strength and thermal stability, biocompatibility and corrosion resistance [1]. However, because of moderate hydride formation enthalpies (ΔH_f=-73 kJ/mol for TiH_2) [2], the Ti-based materials can be susceptible to hydrogen embrittlement when subjected to hydrogen-rich environments under severe operating conditions (e.g., extreme pH levels, high temperatures and pressures). The hard and brittle nature of the hydride precipitation as well as the hydride-induced internal stress concentration leading to mechanical degradation, is a longstanding problem in material science.

Several hydride phases can be found at room temperature corresponding to various amounts of hydrogen, face-centered tetragonal (FCT) TiH, face-centered cubic (FCC) TiH_x (with x ranging between 1.5 and 2) and FCT TiH_2 [3–7]. The FCC phase (δ phase) is the most stable and prevalent hydride. Four types of orientation relationships (ORs) between hexagonal close packed (HCP) matrix and FCT and FCC hydrides have been reported in refs [3–6], which are shown in Table 1. In our previous work [8], the hydride layers formed on the electrolytic hydrogen charging surface were observed for the first time, which mainly obeyed OR1 or OR2 with α-Ti matrix and are strongly dependent on the parent grain orientation. However, the investigation on the mechanical property evolution of diffusion surface during hydride precipitation are missing and significant to be explored.

Table 1 Four orientation relationships of α-Ti / δ-hydride transition.

	Orientation relationship	Interface plane
OR1	{0001}//{1$\bar{1}$1} (angle of 4°), <1$\bar{2}$10>//<110>	{10$\bar{1}$3}//{1$\bar{1}$0}
OR2	{0001} //{001}, <1$\bar{2}$10>//<110>	{10$\bar{1}$0}//{1$\bar{1}$0}
OR3	{10$\bar{1}$1}//{1$\bar{1}$1}, <1$\bar{2}$10>//<110>	{0001}//{1$\bar{1}$2}
OR4	{$\bar{1}$011}//{001}, <1$\bar{2}$10>//<110>	{10$\bar{1}$1}//{1$\bar{1}\bar{1}$}

Grain size effect on hydride precipitation in Zircaloy-4 plate has been studied by Wang et al. [9], more intergranular hydrides were found in the fine grain sample with higher density of preferential nucleation sites, that is, grain boundary (GB). The hydride precipitation at grain boundary can produce orientation gradients in the adjacent grain [9] resulting in the nucleation of cross-boundary hydride via an auto-catalytic mechanism [10,11] which related to the collective shear on the slip plane in both grains and the grain boundary energy. Silva et al. [12] proposed that hydride precipitation at grain boundary is directional, probably due to the different grain misorientation angle. The response of different hydride variants to the GB

nucleation also depends on the geometric relationship between GB plane orientation and hydride growth direction. When the effective growth direction of the hydride macro-platelet is aligned with the grain boundary plane orientation, the hydride variant-GB interaction can be synergistic [13]. All the above interaction mechanisms are between GB and Zr-hydride formed under furnace cooling process, which will be taken as significant references on the reaseach of the GB effect on the formation of hydride diffusion layer in titanium.

In the present paper, mechanical property evolution of titanium surface during electrolytic hydrogen charging is investigated. The surface microstructure evolutions with various diffusion times in the sample with different grain sizes are compared with the help of interrupted in-situ electron backscatter diffraction (EBSD) measurements. The formation mechanism of cross-boundary hydride is further studied by the combination of auto-catalytic mechanism and misfit strain of hydride transformation.

2. Experimental methods

In the current work, the material was rolled commercially pure titanium T40 (ASTM grade 2) sheet with the thickness of 1.5 mm. Samples with different average grain sizes were achieved by different annealing processes: Sample A and Sample B with coarse grain size of ~50 μm was annealed at 800 °C for 3 h; Sample C and Sample D (fine grain sample) with grain size of ~30 μm was annealed at 700 °C for 3 h. The obtained materials were fully recrystallized with a typical split basal texture.

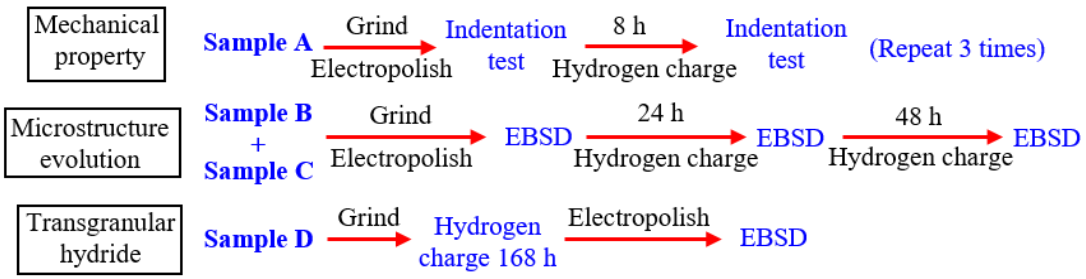

Fig. 1. Schematic diagram of the experimental procedures

The experimental procedures for the four samples are shown in Fig. 1. The samples were ground with SiC papers of grits from 1200# to 2400#. The electrolytic polishing was performed using a solution of 10 vol% perchloric acid in methanol at 35 V, 5 °C for 5 s on the normal direction (**ND**) surface (diffusion surface) of Sample B and Sample C and 30 V, 5 °C for 1 s on Sample D for orientation detection. Hydrogens were introduced into **ND** surface by an

electrolytic method [8] in an electrolyte consisting of 1/3 volume phosphoric acid and 2/3 volume glycerin under an applied current density of 2 kA/m^2.

During hydrogen charging, hydride diffusion layer was gradually formed and cover the entire sample surface. Nanoindentation test was employed to measure the mechanical property evolution of diffusion surface. The indentation hardness (H_{IT}) and plane strain modulus (E^*) were extracted from the unloading part of load-depth curves by using Oliver and Pharr model [14]. Somekawa and Mukai [15] proposed the different deformation behaviors between grain boundary and grain interior. Thus, the coarse-grained Sample A was chosen for the nanoindentation experiment to reduce the influence of grain boundaries on the measured results. The nanoindenter NHT_2 from Anton Paar and Berkovich tip indenter (142.3°) were used with maximum load of 10 mN and loading/unloading rate 20 mN/min. 20×20 indentation matrices with spacing of 20 μm were randomly pressed on the initial surface and hydrogenated surface after every 8 h charging until 24 h. The average hardness and modulus are calculated according the 400 nano-hardness points of each sample.

The interrupted in-situ microstructures of Sample B and Sample C with different grain sizes were performed and compared under EBSD measurement. Pre-charged sample surface was treated for orientation detection, and enough indexation rate can be maintained after charging and will not be reduced too much by the electrolyte. To follow the microstructure evolution of the same zone, the zone of interest was marked by micro-indentation. The microstructures of hydride layer were examined after hydrogen charging for 24 h and 72 h, respectively. The selection of the two charging times will be further explained in Section 3.2. For doing statistical analysis on phase evolution, the hydride layer was indexed by both FCT γ-hydride (a_γ = 0.420 nm, c_γ = 0.470 nm) and FCC δ-hydride (a_δ = 0.440 nm). To study cross-boundary hydride, the hydride platelet in the fine-grained Sample D with larger volume fraction of grain boundary was observed. The hydride platelets can be regarded as hydride nucleation process [8], which can be obtained by removing the thin hydride layer from sample surface via 1s electrolytic polishing, as shown in Fig. 1. Only FCC δ-hydride was chosen as indexed phase for hydride platelet characterization due to that almost all the hydrides have transformed into FCC phase after 168 h hydrogenation.

EBSD characterization was performed using JSM 6490 SEM and JEOL 6500F field emission gun microscopy equipped with an EBSD camera. The Aztec software package (Oxford Instruments) was employed for data acquisition. JSM 6490 SEM was used to make EBSD measurements in large area at a step size of 0.8 μm. Specifically, EBSD patterns were

acquired on a JEOL 6500F field emission gun for obtaining more detailed examinations of and cross-boundary hydride at a step size of 0.1 μm.

3. Result

3.1 Mechanical property of α-Ti at different hydrogen charging times

During hydrogen charging, hard hydride phase precipitates when hydrogen concentration is supersaturated changing the surface properties of α-Ti. Fig. 2 shows the evolution of indentation hardness (H_{IT}) and plane strain modulus (E^*) during hydrogen charging measured by nanoindentation test. Before hydrogen charging, the mean nanohardness and modulus obtained from 400 indents are 2.8±0.3 GPa and 142.1±5.6 GPa, respectively, which coincide with the normal indentation properties of commercial pure titanium (CP-Ti) [16]. With hydrogen charging, the hardness of the sample clearly tends to increase while the modulus decreases. The gradual evolution of hydrogen-induced hardening and elastic modulus reduction is due to the formation of titanium hydride. However, the hardness and elastic modulus tend to maintain a constant level after 16 h of hydrogen charging time, respective 3.7±0.4 GPa and 130.9±6.8 GPa. With the growth of hydride precipitation, the sample surface is gradually covered by hydride layer, then the nanohardness and modulus are unchanged.

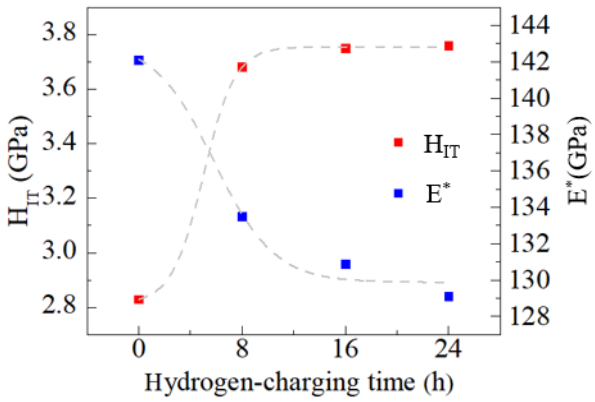

Fig. 2. Hardness (H_{IT}: red) and modulus (E^*: blue) of Sample A depending on hydrogen-charging time

The results are consistent with the previous work of Xu et al. [17], in which the indentation was performed on the cross section of hydride layer, and the hardness was found to be about 30% higher than Ti matrix. The increased hardness of post-charged titanium surface shows the hard nature of hydride layer and thus the poor plastic deformability. Besides, the hydride has a slightly lower modulus than Ti matrix. The reduced E^* means the lower resistance of hydride layer to elastic (recoverable) deformation under indentation load. Setoyama et al. [18] also found that Ti hydride is elastically softer than matrix and the elastic modulus is dependent on

the hydrogen content. By using acoustic emission technique, Shi et al. [19] found that the micro-cracks in hydride can be initiated below the yield strength of Zr alloy and the stresses for crack initiation depend on the hydride length. During elastic deformation, the initiated micro-cracks can result in the reduction of macroscopic elastic modulus [20]. Thus, the formation of defects, such as micro-cracks or void, on the hydride layer can be the reason for the reduced elastic modulus of post-charged surface.

3.2 The microstructure evolution of hydride layer

According to the nanoindentation test, the almost unchanged nanohardness and modulus after 16 h hydrogen charging indicates the formation of hydride diffusion layer. Thus, to observe the microstructure evolution of hydride layer, the sample surface before and after hydrogen charging for 24 h (at the beginning of hydride layer formation) and 72 h (stable hydride layer) were examined. The different results of Sample B (coarse-grained) and Sample C (fine-grained) are shown in Fig. 3 and will be compared in this section.

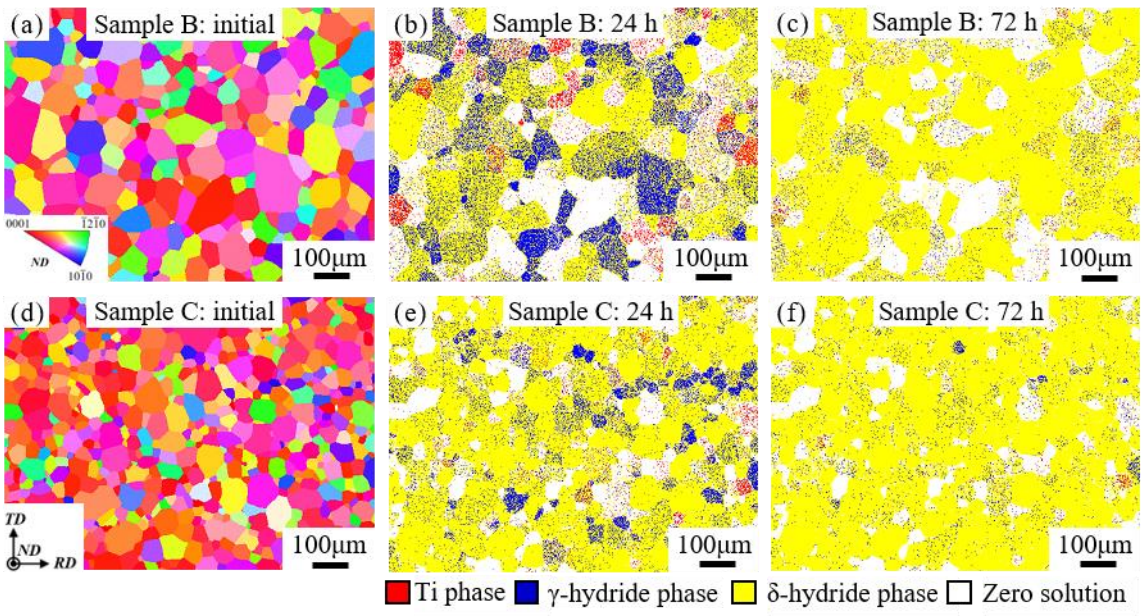

Fig. 3. (a) IPF map of initial grains in Sample B with coarse grain. (b) Phase map after hydrogen charging for 24 h. (c) Phase map after hydrogen charging for 72 h. (d) IPF map of initial grains in Sample C with fine grain. (e) Phase map after hydrogen charging for 24 h. (f) Phase map after hydrogen charging for 72 h. In the phase maps, red: Ti matrix, blue: γ-hydride, yellow: δ-hydride, white: zero solution.

The initial microstructures are shown in Fig. 3a and d in form of inverse pole figure (IPF) maps, where **ND** is projected with the shown color bar (see subgraph in Fig. 3a). After hydrogen charging for 24 h, nearly whole titanium matrix has been transformed into hydride precipitates (γ- and δ-hydride). The fraction of Ti matrix and γ-hydride are much higher in the coarse-

grained Sample B (Fig. 3b) than that in the fine-grained Sample C (Fig. 3e), indicating a facilitating effect of grain boundaries on the formation of δ-hydride. After 72 h, almost all the remnant Ti matrix and γ-hydride are transformed into δ-hydride (as shown in Fig. 3c and f), revealing that the FCC δ-hydride has the highest stability during room temperature hydrogen charging. Noting that, certain grains in the phase maps are always non-indexed because of large lattice distortion. The fact that zero solutions always appear in the grains with *c*-axis nearly parallel to the hydrogen diffusion direction has been explored in [8]. Inside such grains, Kikuchi patterns are too blur to be detected due to the multi-directional deformation and complicated phase boundaries of multiple hydride variants.

In order to clarify the phase evolution process of hydride layers during hydrogen charging, the phase components in Sample B and C are further plotted in form of bar chart (Fig. 4) according to the data from EBSD measurements. In Fig. 4, red label refers to Ti matrix, while yellow and blue are δ-hydride and γ-hydride respectively, white is zero solution. Before hydrogen charging, there appears single Ti phase in both samples.

The evolution of Sample B is observed first. After hydrogen charging for 24 h, close to 100% of the Ti phase has transformed into hydrides (γ and δ phase) and/or non-indexed areas. Due to the highest stability, the FCC δ-hydrides occupy the majority of the diffusion surface rapidly during hydriding process, the surface fraction of δ phase (45%) is much higher than that of γ-phase (13%) after 24 h charging. The proportion of δ-hydride continually increases with further hydrogen atoms diffusion, consuming the γ-hydride phase. After 72 hours, γ-hydride nearly disappears and the diffusion surface consists of only δ-hydride and non-indexed areas. According to the observation, metastable γ-hydrides can be firstly formed under the chemical force driven by the high hydrogen concentration in the titanium matrix, but gradually transformed into the stable FCC structure over time.

Phase evolution of Sample C (fine-grained) is also examined to study the effect of grain size on the hydride transition process, as shown in Fig. 4. During hydrogen charging, Sample C follows the similar phase evolution tendency to that of Sample B, while showing significant difference on the proportion of each phase. Compared to Sample B, more δ-hydride, but less remnant Ti matrix and γ-hydride are observed in Sample C after charging for 24 h, indicating that the phase transformation process from Ti to stable δ-hydride is faster in Sample C, due to the higher volume fraction of grain boundaries in the fine-grained sample. The stable δ-hydride can be regarded as the saturation state of surface diffusion, thus the hydrogen saturation time of the fine-grained Sample C should be shorter. Furthermore, the lower fraction of non-indexed

area is observed inside fine-grained Sample C, indicating the reduced distortion of hydride transformation.

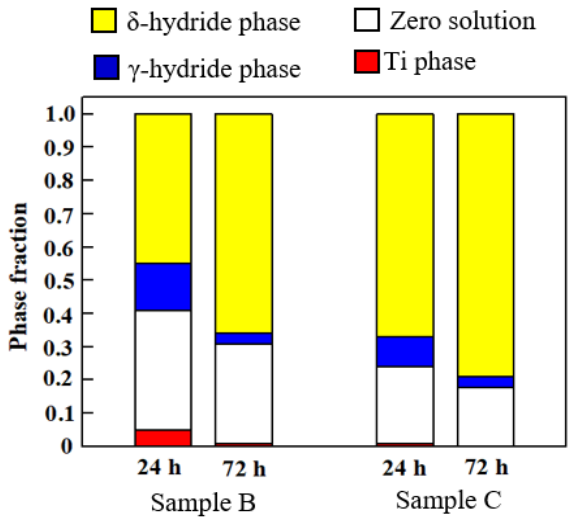

Fig. 4. Evolution of phase composition during hydrogen charging in Sample B and Sample C.

The grain boundaries are believed to be fast diffusion path for hydrogen with significant higher diffusion coefficient [21]. Thus, Sample C with larger volume of grain boundaries has faster hydrogen adsorption rate and shorter saturation time. Besides, the nucleation of hydrides tends to be preferential at grain boundaries because of the high interface energy and relatively weak bonding. Indeed, more hydrides are detected at grain boundaries in fine-grained material [9]. The high density of defects at grain boundary is also favorable to accommodate the misfit strain of hydride transition.

3.3 Cross-boundary hydride

According to the previous work of Wang et al. [8], free surface relaxation is the dominated macro accommodation mechanism for hydride transformation during hydrogen diffusion. In addition, our results above show that micro accommodations by grain boundary also play an important role. According to Fig. 3, hydride transformation is faster in fine-grained sample because of increased grain boundary area, where is energy favorable for priority hydride nucleation. Thus, fine-grained Sample D was chosen to further research grain boundary accommodation during hydride nucleation. After polishing out the hydride layer, hydride platelets occur on the diffusion surface (**ND** surface), as shown in Fig. 5. Fig. 5a shows IPF map, both hydride and titanium are colored by **ND**, while corresponding phase map with colored boundaries is presented in Fig. 5b. Hydrides phase mainly follows OR1 with the surrounding matrix, because the texture of **ND** diffusion surface is favorable for OR1

transformation [8]. Some $\{10\bar{1}2\}$ tension twins labeled by green lines occur at hydride interface, which can be induced by the misfit strain of hydride transformation. The accommodation mechanism of hydride-twin pair will be investigated in our future work.

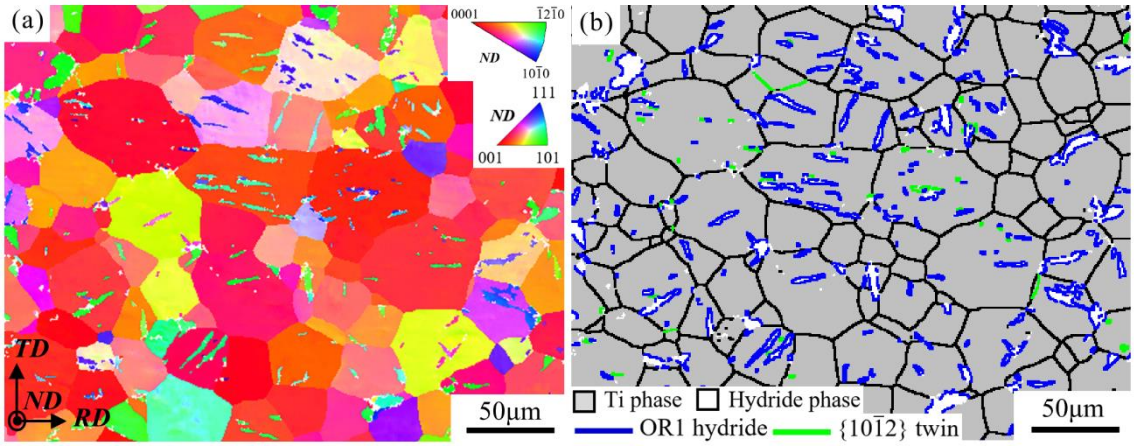

Fig. 5. (a) IPF map of hydride platelets in Sample D. (b) EBSD map to show the $\{10\bar{1}2\}$ twin boundary and OR1 hydride phase boundary. All the indexed phases are color by gray. Green line shows the twin boundaries of $\{10\bar{1}2\}$ extension twin. Blue line is interface plane of OR1 hydride, respectively. Grain boundaries are colored by black.

Grain boundary induced hydride transmissions are determined in Fig. 5. Wang et al. [9] proposed that, in the neighboring grains, misfit dislocations can be produced adjacent to the tip of intergranular hydride. Thus, hydrides in neighbor grain are induced by preferentially formed intergranular hydride and accommodate the concentrated misfit strain. In this section, the preferred boundary for crossed Ti-hydride formed by electrolytic hydrogen charging is explored. Firstly, the ***c***-axis misorientation angles (θ_c) of 200 random grain boundaries selected from Fig. 4 are calculated to reveal the intrinsic ***c***-axis misorientation distribution of the textured plate. After that, θ_c of 210 hydride-crossed boundaries are obtained for the analysis of boundary preference of hydride transmission. The results are presented in Fig. 6. For the distribution of intrinsic ***c***-axis misorientation (black bars) from 0^o and 90^o, there appear three peaks focus on the angle around 35-40^o, 60-65^o and 85-90^o. Compared with the data set of all boundaries, the peaks of crossed boundaries (red bars) are shifted towards left and right side, respectively. The formation of cross-boundary hydride prefers the grain boundaries with both the low θ_c ($< 30^o$) and the high θ_c ($75^o < \theta_c < 85^o$), while the grain boundaries with the ***c***-axis misorientation angle between 30^o and 75^o and larger than 85^o are unfavorable. The reason will be further discussed.

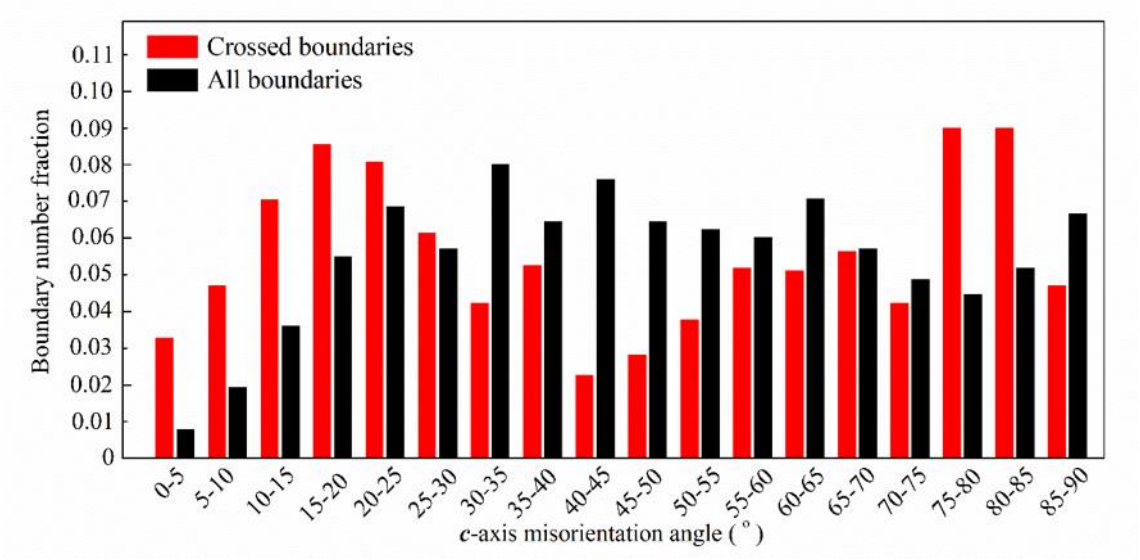

Fig. 6. EBSD-based distribution of grain boundaries and hydride crossing at grain boundaries with ***c***-axis misorientation angle.

There appears an abnormal decrease of boundary fraction at high θ_c value of 85-90° in Fig. 6. During the statistics of hydride-crossed boundary, to ensure the accuracy, the identified cross-boundary hydrides must be more than 5 pixels in Fig. 5. With the increase of ***c***-axis misorientation, the grain orientations can deviate from the favorable orientation for hydride nucleation leading to the small size of crossed hydride. The excluded hydrides less than 5 pixels finally result in the decrease of crossed hydride at 85-90° θ_c boundary. However, according to the tendency at 75-85°, it can be speculated that the actual number of crossed hydride at 85-90° boundary is larger than the calculated value.

The details of hydride transition at low angle and high angle grain boundaries are shown in Fig. 7a and b. The disorientation angle is 10.2° between Grain 1 and Grain 2, while 82.9° between Grain 3 and Grain 4. For convenience, B_i is employed to denote the six OR1 hydride variants (i=1,2,3…6) as listed in Table 2. The OR1 hydride variants were defined by the interface planes with corresponding shear of Shockley dislocation. In the pole figures, the selected hydride variant in each grain is marked by the red circle. The hydride variant selection follows the principle studied in [8], which is not influenced by the neighboring hydride and grain boundary. The selected OR1 variant are always the most favorable one to accommodate the misfit strain of hydride transformation with the $\{10\bar{1}3\}$ interface plane closest to hydrogen diffusion surface. Thus, it can be inferred that, when the grains at both sides of boundary have preferential orientation for OR1 transformation, the nucleation probability of cross-boundary

hydride is higher. On the contrary, hydride transmission is restrained if the neighboring grain orientation is unfavorable.

Table 2 Variants of OR1 hydride

	Variant 1	Variant 2	Variant 3	Variant 4	Variant 5	Variant 6
OR1 hydride (B_i)	B_1 $(10\bar{1}3)[10\bar{1}0]$	B_2 $(01\bar{1}3)[01\bar{1}0]$	B_3 $(\bar{1}103)[\bar{1}100]$	B_4 $(\bar{1}013)[\bar{1}010]$	B_5 $(0\bar{1}13)[0\bar{1}10]$	B_6 $(1\bar{1}03)[1\bar{1}00]$

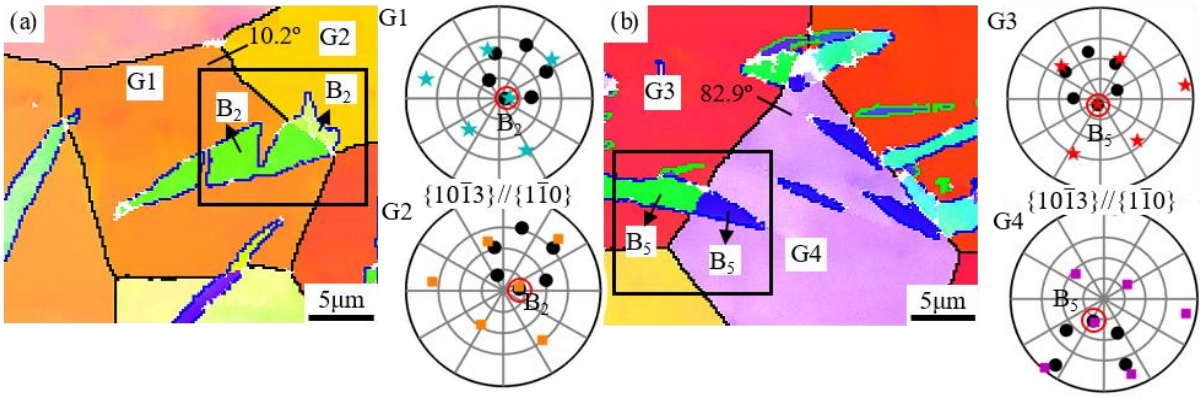

Fig. 7. IPF map of cross-boundary hydride **(a)** at low angle boundary (Grain 1 and Grain 2) and **(b)** high angle boundary (Grain 3 and Grain 4). The black dots represent the $\{10\bar{1}3\}$ interface planes of Ti matrix and the colors represent the $\{1\bar{1}0\}$ interface planes of hydrides. The twin, grain and OR1 hydride boundaries are colored by green, black and blue, respectively. (Euler angle of G1: 145.9° 35.9° 53.6°, G2: 149.3° 40.4° 59.6°, G3: 21.1° 155.6° 42.8, G4: 167.7° 120.5° 18.5°)

4. Discussion

Hydride transformation (OR1), similar to a martensitic transformation, consists of a shear deformation on basal plane and a lattice expansion, while twinning is a pure shear deformation mode. The twin transmission at grain boundary has already been investigated in-depth [22]. Thus, before the discussion of hydride transmission, twinning can be considered as a reference. Kumar et al. [22] suggested that twin transmission frequency in HCP materials decreases with the increase of grain boundary misorientation, which is commonly attributed to the misalignment in the twin plane and shear direction at the grain boundary with large misorientation. The tendency of twin transmission frequency should be nearly the same when grain boundary misorientation is replaced by ***c***-axis misorientation angle used in this paper.

Specially, the frequency of hydride transmission is not monotonically decreasing with the increased ***c***-axis misorientation, as shown in Fig. 6, where the peaks occur on both low and high angle regions. The hydride transmission has also been investigated in zirconium when hydride nucleates during moderately slow cooling process [9]. The precipitation of cross-boundary

hydride favors the grain boundaries with both the low θ_c (< 40°) and the high θ_c (> 80°), which is slightly different from our results, the low θ_c (< 30°) and the high θ_c (75° < θ_c < 85°), probably due to the different materials or hydriding process (electrolytic hydrogen charging in our work).

The favorable hydride transmission in low θ_c boundary is mainly due to the shear accommodation like the transmission of twin. The shear inside the formed hydride platelet results from the 1/3 $<10\bar{1}0>$ Shockley partial dislocation. The alignment of slip planes and slip directions ($\{0001\}$ and $<1\bar{1}00>$) at the grain boundary are responsible for the hydride transmission. For any grain boundary, the $<1\bar{1}00>$ misorientation angle is always low, allowing for easy collective shear [9]. Thus, the alignment of $\{0001\}$ plane is of particular importance and responsible for the preferable hydride transmission in low θ_c range. The analysis should be associated with the auto-catalytic mechanism for the growth of cross-boundary hydride proposed by Wang et al. [9]. For low θ_c boundaries, basal slip can be easily induced by the strain misfit produced by hydride tip in the neighbor grain with aligned slip plane ($\{0001\}$ basal plane). Solute hydrogen atoms nearby tend to diffuse towards the dislocated area, that is, chemical potential well. The chemical stress accompanying hydrogen agglomeration stimulates the dissociation of 1/3 $<11\bar{2}0>$ dislocations into 1/3 $<10\bar{1}0>$ partial dislocations [23] and then the hydride nucleation occurs across the grain boundary. Besides, the angles between the two shear plane intersections with the grain boundary plane are also effective factors for the slip transmission [24], which is difficult to be evaluated in experiment by non-destructive manner.

The effect of shear on hydride transmission is weakened with the increase of ***c***-axis misorientation angle. The again appearance of strong intensity of hydride transmission at high θ_c grain boundaries confirms that the cross-boundary hydride should not only induced by the pure shear accommodation like twin transmission. Indeed, as mentioned before, OR1 hydride transformation contains both shear misfit and large dilatation along ***c***-axis. Thus, for the hydride transmission at high θ_c boundary, ***c***-axis dilatation difficult accommodated by misfit dislocations should be regarded as the major factor. Prismatic slip $\{10\bar{1}0\}<1\bar{2}10>$ is the dominant slip family at room temperature in α-titanium [25]. Carpenter [23] proposed that the 1/3 $<10\bar{1}0>$ Shockley dislocation for OR1 hydride nucleation can be dissociated from a screw segment of prismatic dislocation by chemical stress accompanying hydrogen agglomeration. Thus, the stimulation of prismatic slip is speculated as another important part for the hydride nuclear reaction.

Schmid factor (SF) criterion is used to evaluate the probability of slip activation in Grain A under the effect of ***c***-axis dilatation in neighbor grain (Grain B), which is equivalent to a uniaxial compressive stress for Grain A. Under uniaxial stress, the SF of prismatic slip in Grain A can be obtained by the stress projection on the slip systems:

$$SF = \cos(\theta)\cos(\lambda) \quad (1)$$

where θ is the angle between slip plane normal $<10\bar{1}0>$ and stress direction, and λ shows the angle between slip direction $<1\bar{2}10>$ and stress direction [26]. The different types of grain boundaries can be obtained by manipulating the Euler angle of Grain A using the method of Wang et al. [9]. The $[\varphi_1, \phi, \varphi_2] = [90^o, 90^o, 0]$ is taken as reference Euler angles of neighbor Grain B, while three types of initial orientations are taken for Grain A: Type I $[90^o, 90^o, 0]$ (red square), Type II $[90^o, 90^o, 15^o]$ (black round) and Type III $[90^o, 90^o, 30^o]$ (blue star), of which ***c***-axes are all aligned to that of Grain B. Grain A is misoriented through altering the angle ϕ (rotation around $[10\bar{1}0]$) from 90º to 0º, in which the SFs for prismatic slip systems are calculated every time ϕ goes down 5^o.

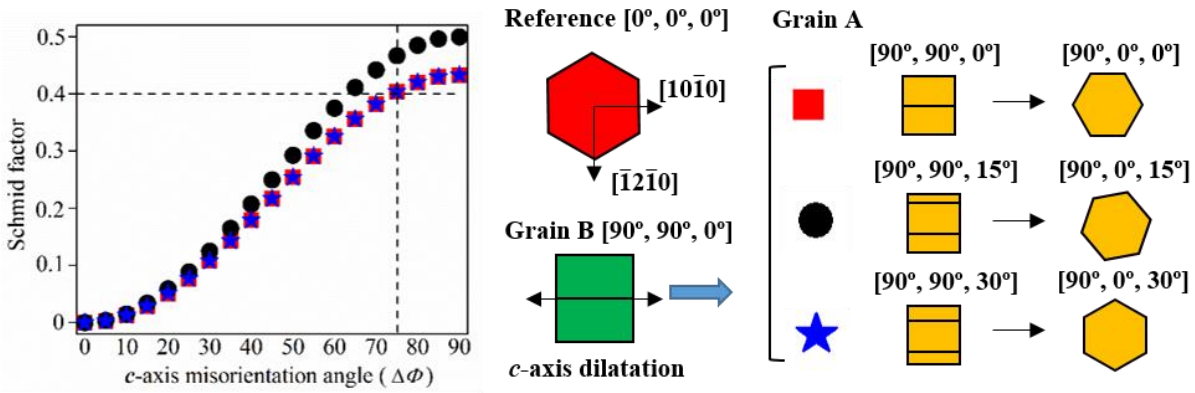

Fig. 8. Change in the Schmid factor of prismatic slip system as a function of ***c***-axis misorientation.

The maximum SFs corresponding to $\Delta\phi$ (***c***-axis misorientation between Grain A and Grain B) are shown in Fig. 8, indicating increased SFs with the increase of $\Delta\phi$ in all types of Grain A. Due to the symmetry of HCP crystal, the SFs for Type I and Type III Grain A are the same, while increase faster up to 0.5 (the maximum of SF) for Type II Grain A. Especially, when ***c***-axis misorientation is higher than 75^o, all the SFs are larger than 0.4, indicating the easier activation of prismatic slip. Above all, high frequency hydride transmission at high θ_c grain boundaries can be due to higher activity of prismatic slip near the neighboring hydride tip. In addition, the high θ_c grain boundaries with higher energy can also as the preferential position of hydride nucleation during hydrogen diffusion.

5. Conclusion

The hydride precipitation formed by electrolytic hydrogen charging on **ND** surface of CP-Ti mainly follows the orientation relationship of $\{0001\}//\{1\bar{1}1\}\ <1\bar{2}10>//<110>$ with Ti matrix. The hardness of charged surface clearly tends to increase while modulus decreases until 16 h charging, after that, both of them maintain a constant level. The hydrogen-induced hardening and elastic modulus reduction are mainly due to the formation of hydride precipitation. The microstructure evolutions of the sample with different grain sizes are compared with the help of interrupted in-situ EBSD measurements. In the fine grain sample, more grain boundaries result in the faster hydride transformation from γ to stable δ hydride and less distortion than large grain sample. The formation of cross-boundary hydride is a kind of grain boundary accommodation mechanism. Cross-boundary hydrides prefer to be formed at the grain boundary with both the low θc ($< 30^o$) and the high θc ($75^o < \theta c < 85^o$). The reason for the preference at low θ_c boundaries is the aligned {0001} slip plane of adjacent grains. The high activity of prismatic slip under ***c***-axis dilatation of neighbor grain can result in the amount of hydride transmissions at the high θ_c boundaries ($75^o < \theta c < 85^o$).

Declaration of interests

The authors declare that they have no known competing financial interests or personal relationships that could have appeared to influence the work reported in this paper.

Acknowledgements

The authors would like to thank Prof. Eric Fleury for the loan of the hydrogen charging device. The first author Qian Wang is grateful to the China Scholarship Council for the support of her PhD study in France.

References

[1] D. Banerjee, J.C. Williams, Perspectives on titanium science and technology, Acta Mater. 61 (2013) 844–879.
[2] A. Andreasen, Predicting formation enthalpies of metal hydrides, 2004.
[3] E. Conforto, D. Caillard, A fast method for determining favourable orientation relationships and interface planes: Application to titanium-titanium hydrides transformations, Acta Mater. 55 (2007) 785–798.
[4] A. Bourret, A. Lasalmonie, S. Naka, In-situ high resolution observation of hydride precipitation in titanium, Scr. Metall. 20 (1986) 861–866.
[5] H. Numakura, M. Koiwa, Hydride precipitation in titanium, Acta Metall. 32 (1984) 1799–1807.
[6] E. Conforto, D. Caillard, Edge-to-edge matching at Ti-TiH interfaces: kinetics of hydride growth and clustering of precipitates with different orientation relationships, Solid State Phenom. 172–174 (2011) 242–247.
[7] O.T. Woo, G.C. Weatherly, C.E. Coleman, R.W. Gilbert, The precipitation of γ-deuterides (hydrides) in titanium, Acta Metall. 33 (1985) 1897–1906.
[8] Q. Wang, S. Xu, J.S. Lecomte, C. Schuman, L. Peltier, X. Shen, W. Song, Crystallographic orientation dependence of hydride precipitation in commercial pure titanium, Acta Mater. 183 (2020) 329–339.

[9] S. Wang, F. Giuliani, T. Ben Britton, Microstructure and formation mechanisms of δ-hydrides in variable grain size Zircaloy-4 studied by electron backscatter diffraction, Acta Mater. 169 (2019) 76–87.
[10] J.S. Bradbrook, G.W. Lorimer, N. Ridley, The precipitation of zirconium hydride in zirconium and zircaloy-2, J. Nucl. Mater. 42 (1972) 142–160.
[11] V. Perovic, G.C. Weatherly, C.J. Simpson, Hydride precipitation in α/β zirconium alloys, Acta Metall. 31 (1983) 1381–1391.
[12] C.M. Silva, F. Ibrahim, E.G. Lindquist, J.W. McMurray, C.D. Bryan, Brittle nature and the related effects of zirconium hydrides in Zircaloy-4, Mater. Sci. Eng. A. 767 (2019) 138396.
[13] W. Qin, N.A.P. Kiran Kumar, J.A. Szpunar, J. Kozinski, Intergranular δ-hydride nucleation and orientation in zirconium alloys, Acta Mater. 59 (2011) 7010–7021.
[14] W.C. Oliver, G.M. Pharr, Measurement of hardness and elastic modulus by instrumented indentation: Advances in understanding and refinements to methodology, J. Mater. Res. 19 (2004) 3–20.
[15] H. Somekawa, T. Mukai, Nanoindentation creep behavior of grain boundary in pure magnesium, Philos. Mag. Lett. 90 (2010) 883–890.
[16] C. Fizanne-Michel, M. Cornen, P. Castany, I. Péron, T. Gloriant, Determination of hardness and elastic modulus inverse pole figures of a polycrystalline commercially pure titanium by coupling nanoindentation and EBSD techniques, Mater. Sci. Eng. A. 613 (2014) 159–162.
[17] J.J. Xu, H.Y. Cheung, S.Q. Shi, Mechanical properties of titanium hydride, J. Alloys Compd. 436 (2007) 82–85.
[18] D. Setoyama, J. Matsunaga, H. Muta, M. Uno, S. Yamanaka, Mechanical properties of titanium hydride, J. Alloys Compd. 381 (2004) 215–220.
[19] S.-Q. Shi, M.P. Puls, Fracture strength of hydride precipitates in Zr–2.5 Nb alloys, J. Nucl. Mater. 275 (1999) 312–317.
[20] F.C.S. Carvalho, J.F. Labuz, Experiments on effective elastic modulus of two-dimensional solids with cracks and holes, Int. J. Solids Struct. 33 (1996) 4119–4130.
[21] J. Yao, J.R. Cahoon, Theoretical modeling of gain boundary diffusion of hydrogen and its effect on permeation curves, Acta Metall. Mater. 39 (1991) 111–118.
[22] M.A. Kumar, I.J. Beyerlein, R.J. Mccabe, C.N. Tome, Grain neighbour effects on twin transmission in hexagonal close-packed materials, Nat. Commun. 7.1 (2016) 1–9.
[23] G.J.C Carpenter, The precipitation of γ-hydride plates in zirconium, Acta Metall. 29 (1978) 501.
[24] T.R. Bieler, P. Eisenlohr, C. Zhang, H.J. Phukan, M.A. Crimp, Grain boundaries and interfaces in slip transfer, Curr. Opin. Solid State Mater. Sci. 18 (2014) 212–226.
[25] L. Wang, R.I. Barabash, Y. Yang, T.R. Bieler, M.A. Crimp, P. Eisenlohr, W. Liu, G.E. Ice, Experimental Characterization and Crystal Plasticity Modeling of Heterogeneous Deformation in Polycrystalline α-Ti, Metall. Mater. Trans. A. 42 (2011) 626–635.
[26] G.M. Hommer, A.L. Pilchak, A.P. Stebner, Normalized resolved shear stress calculations for single crystals subjected to multiaxial loading, Materialia. 2 (2018) 53–57.